Dalton Transactions

Polymorphism in A3MF6 (A = Rb, Cs; M = Al, Ga) Grown using Mixed Halide Fluxes

Journal:	*Dalton Transactions*
Manuscript ID	DT-ART-02-2023-000352.R2
Article Type:	Paper
Date Submitted by the Author:	18-May-2023
Complete List of Authors:	Morrison, Gregory; University of South Carolina, Chemistry and Biochemistry Masachchi, Lakshani; University of South Carolina, Chemistry and Biochemistry Tisdale, Hunter; University of South Carolina, Chemistry Chang, Tieyan; The University of Chicago, NSF's ChemMatCARS Jones, Virginia; University of South Carolina, Chemistry and Biochemistry Zamorano, K; University of South Carolina, Chemistry and Biochemistry Breton, Logan; University of South Carolina, Chemistry; University of South Carolina Smith, Mark; University of South Carolina, Department of Chemistry and Biochemistry Chen, Yu-Sheng; The University of Chicago, Zur Loye, Hans-Conrad; University of South Carolina, Department of Chemistry and Biochemistry

Polymorphism in A_3MF_6 (A = Rb, Cs; M = Al, Ga) Grown using Mixed Halide Fluxes

Gregory Morrison,[a] Lakshani W. Masachchi,[a] Hunter B. Tisdale,[a] Tieyan Chang,[b] Virginia G. Jones,[a] K. Pilar Zamorano,[a] Logan S. Breton,[a] Mark D. Smith,[a] Yu-Sheng Chen,[b] Hans-Conrad zur Loye*,[a]

[a]*Department of Chemistry and Biochemistry, University of South Carolina, Columbia, SC, 29208*
[b]*NSF's ChemMatCARS, The University of Chicago, Lemont, IL, 60439*
*Corresponding author. E-mail: zurLoye@mailbox.sc.edu

Abstract: Single crystals of A_3MF_6 (A = Rb, Cs; M = Al, Ga) were grown from mixed alkali chloride/fluoride fluxes in sealed silver tubes. For Cs_3AlF_6 and Cs_3GaF_6, two polymorphs were observed at room temperature: *m*-Cs_3MF_6 and *o*-Cs_3MF_6. For the two Rb containing compositions, only one room temperature polymorph was observed: *o*-Rb_3AlF_6 and *t*-Rb_3GaF_6, respectively. Simultaneous TGA/DSC and high temperature SCXRD/PXRD were used to study the high temperature behavior of A_3MF_6. The compounds of all four compositions were found to undergo structure transitions upon heating to the same cubic structure type, *c*-A_3MF_6.

Introduction

The A_3AlF_6 (A = alkali metal) system has garnered considerable attention due to cryolite, Na_3AlF_6, serving as a low melting flux in the Hall-Héroult process for Al metal production.[1] The other alkali metal compounds are also known, namely Li_3AlF_6,[2, 3] K_3AlF_6,[4-6] Rb_3AlF_6,[7] and Cs_3AlF_6,[8, 9] and all contain isolated AlF_6 octahedra separated by alkali cations. The entire A_3AlF_6 series is characterized by having phase transitions upon heating to higher symmetry polymorphs, where the low temperature polymorphs consist of AlF_6 polyhedra with different orientations while the AlF_6 octahedra in the high temperature polymorphs all have the same orientation. Many of the A_3GaF_6 compounds have also been studied and exhibit similar behavior.[10-14]

Synthetic cryolite is produced on an industrial scale using several aqueous routes, typically involving HF as a fluorinating agent. Other polycrystalline A_3AlF_6 samples have been synthesized from the melt starting with stoichiometric AlF_3 and AF,[2] via high-energy ball milling,[15] and by hydrothermal synthesis.[16] There has been less work done on the synthesis of single crystals of A_3AlF_6 phases. Namely, Li_3GaF_6 was grown from the melt,[3, 10] Na_3GaF_6 was grown under mild hydrothermal conditions,[12] and Rb_2KAlF_6 was grown via an ammonothermal method.[17]

We have explored the growth of single crystals of A_3MF_6 (A = Rb, Cs; M = Al, Ga) from mixed halide fluxes. The availability of single crystals has allowed us to determine the crystal structures of two new low temperature polymorphs of Cs_3MF_6, *m*-Cs_3MF_6 and *o*-Cs_3MF_6, and a new low temperature polymorph of Rb_3GaF_6, *t*-Rb_3GaF_6, as well as to perform the first single crystal structure determination for *o*-Rb_3AlF_6. Furthermore, we have studied the thermal behavior of each compound via simultaneous TGA/DSC and high temperature SCXRD or PXRD.

Experimental

Synthesis

AlF_3 (BeanTown Chemical, 99%, anhydrous), GaF_3 (BeanTown Chemical, 99.5%, anhydrous), RbCl (Strem, 99.8%), CsCl (VWR, 99%), and CsF (Alfa Aesar, 99%) were used as received. RbF (Strem, 99.8%, anhydrous) was found to be $RbHF_2$ by PXRD analysis. $RbHF_2$, which comes as large chunks, was ground to a powder in a glovebox using a mortar and pestle prior to use. *Caution! $RbHF_2$ releases HF vapor upon heating. HF is corrosive and acutely toxic. HF exposure causes severe burns that may not be immediately painful and may cause permanent injury or death.*

Single crystals of each compound were grown using mixed alkali chloride/fluoride flux. For *m*-Cs_3AlF_6, *o*-Cs_3AlF_6, *m*-Cs_3GaF_6, *o*-Cs_3GaF_6, *o*-Rb_3AlF_6, and *t*-Rb_3GaF_6, 2 mmol of the respective MF_3 (M = Al, Ga) were loaded into a cylindrical silver crucible (1.2 cm diameter x 5.7 cm length) and covered with a mixture of 9 mmol/11 mmol of CsF/CsCl or 7.55 mmol/11 mmol $RbHF_2$/RbCl flux. The tube was then placed in a vacuum drying oven and heated to ~180 ºC to remove any moisture from the reagents. After vacuum heating, the tube was sealed shut by partially crimping the entire headspace of the tube and completely crimping the top ~1 cm of the tube. The top of the tube was then folded over and tightly crimped a second time to produce a cold weld. The sealed tubes were placed in a programmable tube furnace under N_2 flow, rapidly heated to 600 ºC for the two monoclinic phases (*m*-Cs_3AlF_6 and *m*-Cs_3GaF_6), 700 ºC for *t*-Rb_3GaF_6, or 750 ºC for the orthorhombic phases (*o*-Cs_3AlF_6, *o*-Cs_3GaF_6, and *o*-Rb_3AlF_6), and dwelled at this temperature for 12 h before slow cooling to 400 ºC (Cs) or 500 ºC (Rb) at a rate of 6 ºC/h. Once the slow cool was completed, the furnace shut off and was allowed to cool to room temperature. The tubes were then cut open, the flux was dissolved via sonication in methanol, and the remaining products were recovered via vacuum filtration. The resulting crystals were then either immediately analyzed or stored in sealed vials under N_2 for future analysis as the crystals were found to be

slightly hygroscopic. All reactions yielded phase pure, small, colorless crystals of the respective compound.

Structure

Structure determination for all room temperature structures excluding *t*-Rb_3GaF_6 was performed using single crystal X-ray diffraction (SCXRD) data. Data were collected on a Bruker D8 Quest diffractometer equipped with a microfocus Mo Kα X-ray source and a Photon II detector. Data were integrated using SAINT and corrected for absorption effects using SADABS in the APEX3 interface.[18] An initial structure solution for each compound was obtained using ShelXT[19] and refined using ShelXL[20] in the Olex2 interface.[21] All examined crystals of *m*-Cs_3MF_6 were found to be twinned, typically exhibiting pseudomerohedral twinning to appear orthorhombic with different lattice parameters than those for *o*-Cs_3MF_6. The structures reported here are based on data from the least twinned crystals that were found. The TwinRotMat functionality in the Platon program[22] was used to identify the pertinent twin law, 0 0 -1 0 -1 0 -1 0 0. Each structure was refined as a two-component twin with the volume fraction of the smaller twin being 0.0585(13) for *m*-Cs_3AlF_6 and 0.0703(14) for *m*-Cs_3GaF_6. For *m*-Cs_3AlF_6, accounting for this twinning reduced the R_1 from 0.0331 to 0.0244 and decreased the maximum and minimum residual electron density peaks from 6.399/-3.134 to 3.972/-2.069, respectively. For *m*-Cs_3GaF_6, accounting for this twinning reduced the R_1 from 0.0389 to 0.0281and decreased the maximum and minimum residual electron density peaks from 7.954/-3.522 to 4.065/-3.099, respectively. No twinning was observed in crystals of the orthorhombic polymorphs. The structures of *m*-Cs_3MF_6 and *o*-A_3MF_6 consist of isolated MF_6 octahedra. In each case, some of these octahedra are ordered and some have multiple orientations, evidenced by many smaller electron peaks surrounding these M atoms instead of just six main peaks. In *m*-Cs_3AlF_6 and *m*-Cs_3GaF_6, these MF_6 octahedra were modeled to have 3

orientations with reasonable fluorine ADPs, whereas for *o*-Cs_3AlF_6, *o*-Cs_3GaF_6, and *o*-Rb_3AlF_6, the best obtainable model consisted of two orientations with larger, more oblate/prolate fluorine ADPs. To address concerns that the crystal structure did not correctly account for all the twinning, another crystal of *m*-Cs_3GaF_6 was independently solved by a second crystallographer. This model is essentially identical to the one reported here though with slight differences in the modelling of the disorder. A comparison/discussion of the two models is provided in the Supporting Information, including Table S1 and Figure S1. *o*-A_3MF_6 crystallize in a known structure type, the *o*-Rb_3AlF_6 type, whose parent member's structure was determined via structure solution of synchrotron powder X-ray diffraction data, where twinning is not relevant. We therefore did not seek further corroboration of these structures. Crystallographic information for each structure is provided in Table 1. In each case, the maximum and minimum residual electron density peaks/holes were adjacent to the heavy Cs or Rb atoms.

Table 1. Crystallographic data for SCXRD structure refinements of the reported compounds.

Compound	*m*-Cs_3AlF_6	*o*-Cs_3AlF_6	*m*-Cs_3GaF_6	*o*-Cs_3GaF_6	*o*-Rb_3AlF_6	*c*-Cs_3AlF_6
Space group	*C*2/*m*	*Fddd*	*C*2/*m*	*Fddd*	*Fddd*	*Fm*-3*m*
Pearson Symbol	mC120	oF480	mC120	oF480	oF480	cF40
a (Å)	11.2739(2)	13.0311(6)	11.3996(3)	13.1762(8)	12.4412(11)	9.3433(3)
b (Å)	19.5018(4)	18.4837(9)	19.7132(4)	18.7515(12)	17.6466(16)	9.3433(3)
c (Å)	11.3248(2)	39.0240(18)	11.4551(4)	39.488(3)	37.201(4)	9.3433(3)
β (°)	109.6410(10)	90	109.7000(10)	90	90	90
V (Å^3)	2345.02(8)	9399.4(8)	2423.55(12)	9756.4(11)	8167.4(13)	815.64(8)
Z	12	48	12	48	48	4
Crystal size (mm^3)	0.04 x 0.04 x 0.04	0.12 x 0.08 x 0.08	0.04 x 0.04 x 0.04	0.08 x 0.07 x 0.07	0.13 x 0.10 x 0.09	
Temperature (K)	300(2)	300(2)	300(2)	299(2)	299(2)	623(2)
Density (g cm^{-3})	4.586	4.577	4.789	4.758	3.878	4.395
θ Range (°)	2.184 – 33.142	2.438 – 36.365	2.161 – 33.137	2.405 – 36.334	2.190 – 30.504	2.195 – 19.862
μ (mm^{-1})	14.061	14.032	16.760	16.653	21.650	3.106
Data Collection and Refinement						
Collected reflections	108074	222336	102291	215240	133061	11945
Unique reflections	4590	5719	4759	5926	3134	131
R_{int}	0.0374	0.0422	0.0376	0.0403	0.0742	0.1004
h	$-17 \le h \le 17$	$-21 \le h \le 21$	$-17 \le h \le 17$	$-21 \le h \le 21$	$-17 \le h \le 17$	$-15 \le h \le 15$
k	$-30 \le k \le 30$	$-30 \le k \le 30$	$-30 \le k \le 30$	$-31 \le k \le 31$	$-25 \le k \le 25$	$-14 \le k \le 15$
l	$-17 \le l \le 17$	$-64 \le l \le 65$	$-17 \le l \le 17$	$-65 \le l \le 65$	$-53 \le l \le 53$	$-15 \le l \le 15$
$\Delta\rho_{max}$ (e Å^{-3})	3.972	2.432	4.065	1.519	1.712	1.758
$\Delta\rho_{min}$ (e Å^{-3})	-2.609	-2.110	-3.099	-1.920	-0.863	-1.332
GoF	1.165	1.122	1.159	1.104	1.069	1.148
Extinction coefficient	0.000148(14)	0.0000219(15)	0.000159(14)	0.0000116(14)	0.000011(3)	-
[a] $R_1(F)$ for $F_o^2 > 2\sigma(F_o^2)$	0.0244	0.0255	0.0281	0.0264	0.0252	0.0527
[b] $R_w(F_o^2)$	0.0619	0.0565	0.0717	0.0626	0.0643	0.1579

[a] $R_1 = \Sigma||F_0| - |F_c||/\Sigma|F_0|$

[b] $wR_2 = [\Sigma w(F_o^2 - F_c^2)^2/\Sigma w(F_0^2)^2]^{1/2}$; $P = (F_o^2 + 2F_c^2)/3$; $w = 1/[\sigma^2(F_o^2) + (0.0242P)^2 + 18.9315P]$ for *m*-Cs_3AlF_6; $w = 1/[\sigma^2(F_o^2) + (0.0150P)^2 + 163.1195P]$ for *o*-Cs_3AlF_6; $w = 1/[\sigma^2(F_o^2) + (0.0291P)^2 + 25.0230P]$ for *m*-Cs_3GaF_6; $w = 1/[\sigma^2(F_o^2) + (0.0180P)^2 + 173.9705P]$ for *o*-Cs_3GaF_6; $w = 1/[\sigma^2(F_o^2) + (0.0253P)^2 + 96.4949P]$ for *o*-Rb_3AlF_6; $w = 1/[\sigma^2(F_o^2) + (0.0508P)^2 + 28.6465P]$ for *c*-Cs_3AlF_6.

Single crystals of *t*-Rb_3GaF_6 diffracted weakly and were highly twinned. As a result, a suitable single crystal for structure determination was not able to be found. Instead, structure determination was performed using powder X-ray diffraction data collected in reflection geometry on a Rigaku SmartLab Diffractometer equipped with a Cu Kα rotating anode.

Structure determination for *c*-Cs_3AlF_6 was performed via SCXRD at NSF's ChemMatCARS beamline at Argonne National Lab. Data were collected at 350 °C. The raw images were then transferred to a Bruker D8 Quest's computer and processed in the APEX3 program.[18] An initial structural model was determined using ShelXT and then refined using ShelXL[20] in the Olex2 interface.[21, 23] Olex2 was used to calculate the correct anomalous dispersion parameter values (f', f", and mu) for each element at the specific wavelength (**λ** = 0.41328 Å). The transition temperatures of the other analogues exceeded the maximum temperature available at NSF's ChemMatCARS and therefore, SCXRD structure solution of their cubic polymorphs was not possible.

Temperature dependent PXRD data for Cs_3AlF_6 and Cs_3GaF_6 were collected on a Rigaku SmartLab Diffractometer equipped with a Mo Kα rotating anode and an Anton Parr HTK1200N heating stage. Cs_3AlF_6 was loaded into an alumina sample well and collected in reflection geometry. Cs_3GaF_6 was loaded into a fused silica capillary and collected in transmission geometry. Samples were heated stepwise at 50 °C increments far from the expected transitions based on DSC data and at 5 °C increments near the transitions with the temperature stabilized at each temperature prior to data collection. Temperature dependent PXRD data for Rb_3GaF_6 were collected on a Rigaku Ultima IV diffractometer equipped with a Cu Kα X-ray source, an HT 1500 high temperature attachment, and a DteX Ultra detector.

Structure determination for *t*-Rb_3GaF_6, *c*-Cs_3AlF_6, and *c*-Cs_3GaF_6 were performed via Rietveld refinement of PXRD data, Figures S14-S16. The diffraction patterns were analyzed, fitted, and refined with the Rietveld/d-I pattern method using the Rigaku SmartLab Studio II software.[24] For *c*-Cs_3MF_6, the high temperature Cs_3AlF_6 single crystal structure was used as an starting model. The background, lattice parameters, peak profiles (split pseudo-Voigt; U, V, W, ηL0/mL0, ηL1/mL1, ηH0/mH0, and ηH1/mH1), F atomic coordinate, and atomic displacement factors (β) were all consecutively refined. All other atoms are on special positions with fixed atomic coordinates. For *t*-Rb_3GaF_6, the background, lattice parameters, peak profiles (split pseudo-Voigt; U, V, W, ηL0/mL0, ηL1/mL1, ηH0/mH0, and ηH1/mH1), Ga atomic coordinates, and Rb atomic coordinates were all consecutively refined using α-K_3AlF_6 as a starting model. Crystallographic information for the Rietveld refined structures is provided in Table 2. The structure of *c*-Rb_3AlF_6 has been previously reported.[7] The existence of *c*-Rb_3GaF_6 was confirmed based on PXRD indexing. However, structure determination was not possible as the furnace attachment to the Rigaku Ultima IV greatly alters peak intensities in a non-modellable fashion. High temperature PXRD analysis on the Rigaku Smartlab was not possible for this compound due to the strong absorption of Mo Kα X-rays by Rb.

Table 2. Crystallographic data for Rietveld structure refinements of the reported compounds.

Compound	*t*-Rb_3GaF_6	*c*-Cs_3AlF_6	*c*-Cs_3GaF_6
Temperature (°C)	30(2)	350(2)	400(2)
Crystal System	Tetragonal	Cubic	Cubic
Space Group	$I4_1/a$	*Fm*-3*m*	*Fm*-3*m*
Pearson Symbol	tI800	cF40	cF40
a (Å)	19.7947(4)	9.3235(3)	9.44763(11)
c (Å)	35.7471(8)	9.3235(3)	9.44763(11)
R_{wp} (%)	3.11	6.82	5.42
R_p (%)	1.83	5.13	4.03
S	9.8341	1.6129	1.6022
χ^2	96.7099	2.6013	2.5672

Phase purity was checked and phase identity post thermal analysis was determined using PXRD data collected at room temperature. Data were collected on a Bruker D2 Phaser diffractometer equipped with a Cu Kα X-ray source and a LYNXEYE silicon strip detector. Data were analyzed using Jade. PXRD patterns for the six room temperature polymorphs are provided in Figures S17-S22.

Thermal Properties

Thermogravimetric analysis (TGA) and differential scanning calorimetry (DSC) were collected simultaneously up to high temperatures on ~20 mg samples to observe structure transitions and melting/sublimation using a TA Instruments SDT Q600. Samples were heated at 10 ºC/min under N_2 flow. Further data were collected up to lower temperatures on ~70-100 mg of samples to further study the structure transitions using a TA Instruments Discovery SDT 650. Samples were heated at 5 ºC/min to the maximum temperature, dwelled for 5 minutes, and then cooled at 5 ºC/min back to room temperature under N_2 flow.

Results and Discussion

Synthesis

The synthesis, structures, and thermal behavior of the reported compounds are schematically summarized in Figure 1 and discussed herein. The reported compounds were all synthesized from mixed alkali halide fluxes. Flux crystal growth has proven to be an excellent method for the growth of single crystals of many classes of compounds including oxides,[25] sulfides,[26] and intermetallics.[27] Surprisingly, there has been little work on the flux crystal growth of fluorides. Most of this work was performed by Barbara Wanklyn, who reported on the crystal growth of numerous ternary and quaternary alkali transition metal fluorides nearly a half century ago.[28-31] These crystals were

primarily grown from $PbCl_2$ or PbF_2-$PbCl_2$ flux, though ACl, ACl-AF, and ACl-AHF_2 (A = alkali cation) fluxes were also used. All reactions were carried out in tightly covered Pt crucibles in open air.

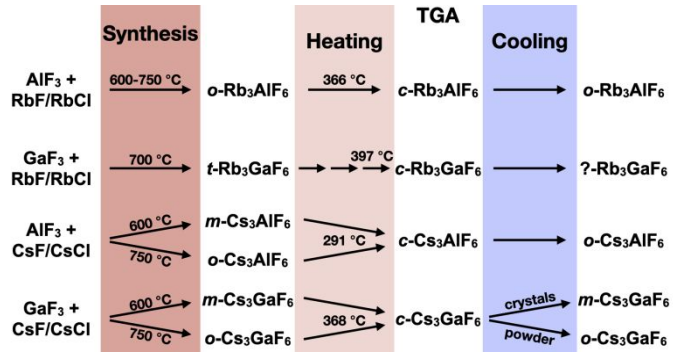

Figure 1. Schematic summary of the synthesis, structures, and thermal behavior of the reported compounds.

Our synthesis method utilized ACl-AF and ACl-HAF_2 fluxes but instead used a crimped shut silver tube crucible to limit the exposure of the fluoride reagents to atmospheric oxygen during heating. Typically, oxygen is eliminated from reactions by sealing the reactions in fused silica tubes. However, fused silica is highly susceptible to attack by fluoride melts and vapors. For this reason, we instead used silver tubes. Vacuum sealing silver crucibles, akin to sealing fused silica tubes, proved impractical, leading us to instead tightly crimp shut the tubes, forming a cold weld. To account for expansion of the air trapped within the tube, which expands to between three and four times its volume at constant pressure when heated to between 600 and 750 °C, the entire tube was partially flattened prior to crimping. The softness of silver then allows the tube to re-expand upon heating to account for the gas expansion. While the air trapped within the tube contains a small amount of oxygen, we did not observe any oxygen impurities in the products. To eliminate any possible oxygen impurities, the tubes can also be crimped within a glovebox.

Silver metal is known to become permeable to oxygen at elevated temperatures.[32] For this reason, we heated the crimped reactions under nitrogen flow within a fused silica tube in a tube

furnace. Conducting the same reactions in a box furnace did not lead to any oxide products, possibly indicating that the tubes we utilized were thick enough to avoid oxygen permeation. However, these reactions did result in the formation of AgCl, which seemingly forms from the flux attacking the inside of the tube coupled with a redox reaction with atmospheric oxygen. While the tubes were crimped shut, they always released a small amount of vapor, representing 1-2 % of the total reaction mass based on weight loss of the tubes, that attacked the inside of the fused silica tube. Although the tubes typically survived this attack, using the same fused silica tube for a second set of reactions resulted in a large amount of unidentified impurity products in the reactions. We have previously found that inserting a metal tube between the reaction vessel and the fused silica tube prevents the degradation of the fused silica tube,[33] however we did not utilize this method here. Tungsten inert gas, TIG, welding shut the tubes was also found to prevent this loss of vapor and we have begun to use this method since.

Structure

The A_3MF_6 compounds all possess structures comprised of isolated MF_6 octahedra separated by A cations. While at high temperatures, all of these MF_6 octahedra have the same orientation, discussed further in the thermal behavior section; at room temperature, a portion of these polyhedra contain a different orientation, with the arrangement of these polyhedra determining the specific structure type.

For Cs_3AlF_6 and Cs_3GaF_6, two room temperature polymorphs are observed. *m*-Cs_3AlF_6 and *m*-Cs_3GaF_6 crystallize in the monoclinic space group *C*2/*m* with lattice parameters a = 11.2739(2) Å, b = 19.5018(4) Å, c = 11.3248(2) Å, and β = 109.6410(10)° at 300(2) K, and a = 11.3996(3) Å, b = 19.7132(4) Å, c = 11.4551(4) Å, and β = 109.7000(10)° at 300(2) K, respectively. The structure, shown in Figure 2, contains columns of MF_6 polyhedra down the *b*-axis. Shown in Figure 2a,

these columns form rows in the *a*-direction. Half of these rows contain only aligned MF_6 polyhedra. In the other half of the rows, every 3rd MF_6 in each column is misaligned and highly disordered across several orientations. As such, one sixth of the MF_6 polyhedra in the structure are misaligned. Shown in Figure 2b, rows of columns along the (2 0 -2) planes all have the same vertical alignment with respect to the *b*-axis. Adjacent rows of columns are shifted vertically such that the polyhedra are between the adjacent polyhedra rows. In other words, if all the polyhedra had the same orientation, they would have a body centered cubic arrangement. An oxide, Sr_3WO_6, exists with similar lattice parameters to *m*-Cs_3MF_6. While structurally related, this compound crystallizes in a different space group, *Cc*, and has a different arrangement of misaligned octahedra.[34]

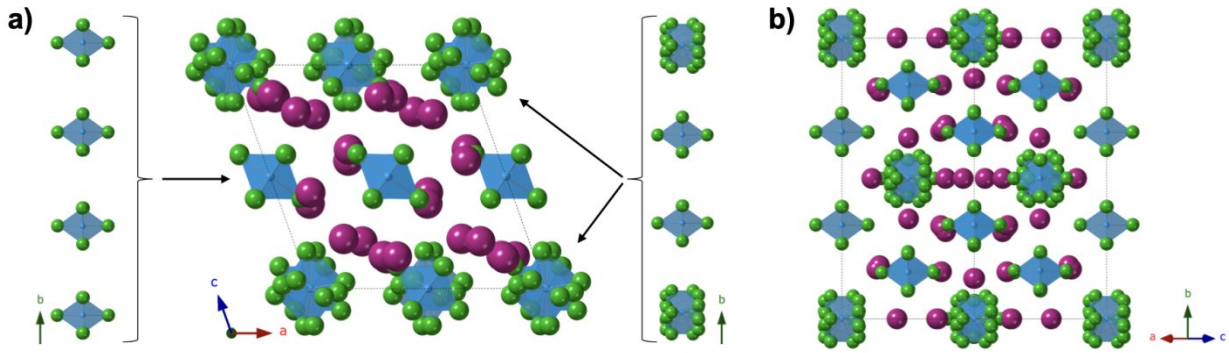

Figure 2. Structure of *m*-Cs_3AlF_6 showing a) the view down the *b*-axis and b) the view down the [1 0 1] direction. Cs atoms are shown in pink, Al polyhedra in blue, and F atoms in green.

The other room temperature polymorphs, *o*-Cs_3AlF_6 and *o*-Cs_3GaF_6, crystallize in the orthorhombic space group *Fddd* with lattice parameters a = 13.0311(6) Å, b = 18.4837(9) Å, and c = 39.0240(18) Å at 300(2) K; and a = 13.1762(8) Å, b = 18.7515(12) Å, and c = 39.488(3) Å at 299(2) K, respectively. The structure, shown in Figure 3, contains similar columns of MF_6 octahedra as in *m*-Cs_3MF_6, this time oriented down the *c*-axis due to the difference in standard axis orders for monoclinic and orthorhombic symmetry. In the orthorhombic polymorph, every 6th polyhedron of every column is misaligned and highly disordered. Figure 4 compares the powder

patterns for the two room temperature polymorphs of Cs_3AlF_6 and clearly indicates the two different structures, *m*-Cs_3AlF_6 and *o*-Cs_3AlF_6.

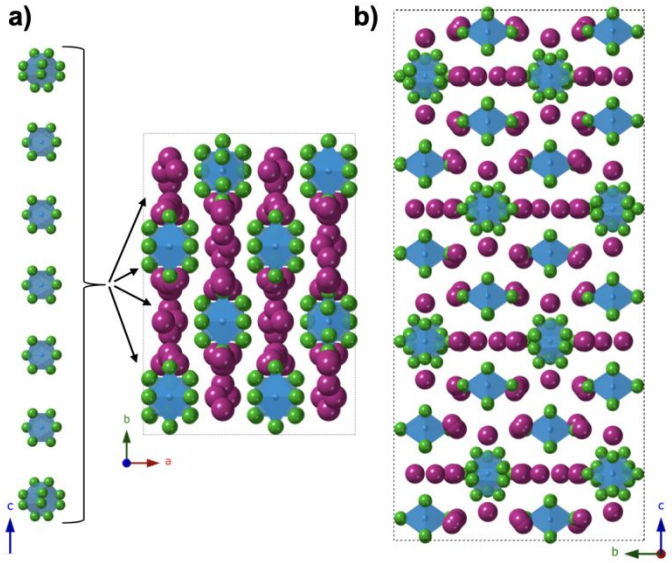

Figure 3. Structure of *o*-Cs_3AlF_6 showing a) the view down the *c*-axis and b) the view down the *a*-axis. Cs atoms are shown in pink, Al polyhedra in blue, and F atoms in green.

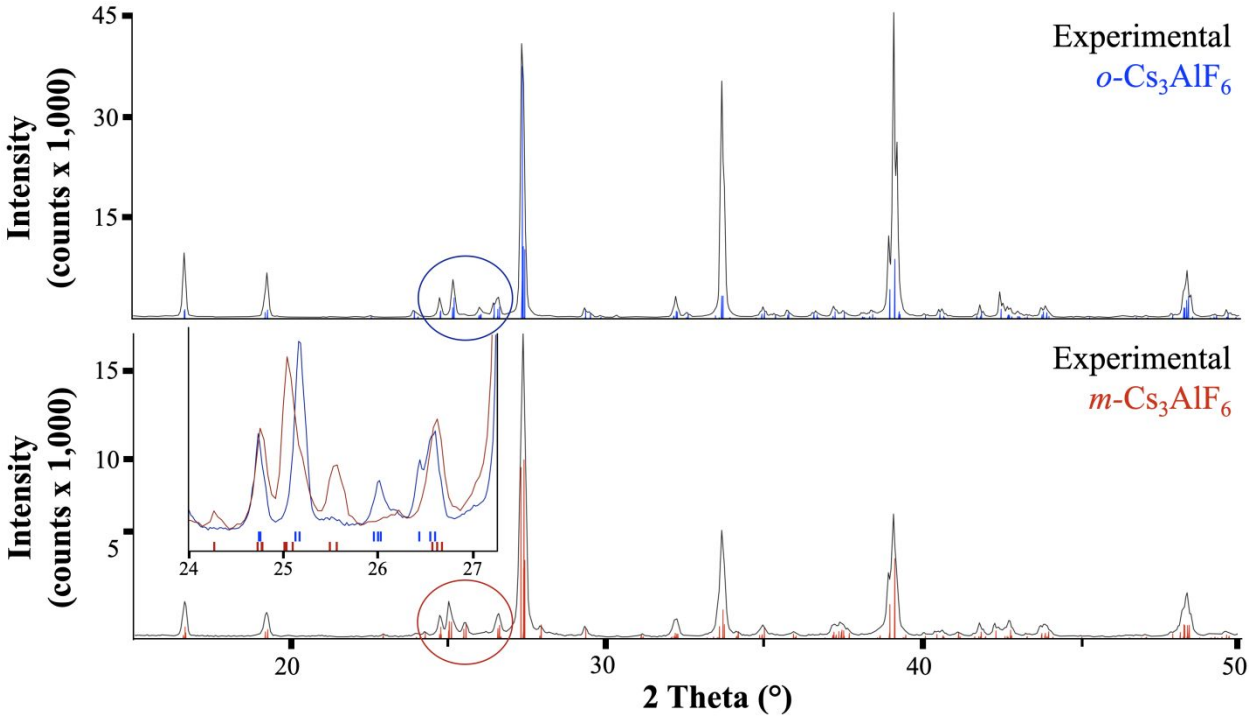

Figure 4. Powder XRD data (Cu K_α) for *m*-Cs_3AlF_6 and *o*-Cs_3AlF_6 showing the experimental data (black) and patterns calculated from the CIFs (colored). The circled regions are zoomed in the inset to highlight one of the differences between the PXRD patterns of the two polymorphs, where *m*-Cs_3AlF_6 consists of a triplet and a singlet of multiplets, whereas *o*-Cs_3AlF_6 consists of two doublets of multiplets. The small peak at 26.2° is the result of W L_α X-rays that arise when the anode of the X-ray tube is contaminated by the W filament. The difference between the calculated and observed intensities for *o*-Cs_3AlF_6 arise from the use of a low-background slide for this data. See Figure S18 for data collected in a well sample holder.

Only one room temperature polymorph was observed for Rb_3AlF_6. *o*-Rb_3AlF_6 crystallizes in the same structure type as *o*-Cs_3MF_6 with lattice parameters a = 12.4412(11) Å, b = 17.6466(9) Å, and c = 37.201(4) Å at 299(2) K. This structure was previously reported based on simulated annealing structure determination and Rietveld refinement of synchrotron powder X-ray diffraction data.[7] The single crystal structure solution is reported here for the first time.

Rb_3GaF_6 also only crystallizes in a single polymorph at room temperature. *t*-Rb_3GaF_6 crystallizes in the α-K_3GaF_6 structure type[14] with space group $I4_1/a$ and lattice parameters a = 19.7947(4) Å and c = 35.7471(8) Å at 303(2) K. The structure, shown in Figure 5, contains columns of isolated GaF_6 octahedra down the *c*-direction separated by Rb cations, akin to the other analogues. However, in *t*-Rb_3GaF_6, there are three different orientations of GaF_6 octahedra. One fifth of the columns contain all one orientation of octahedra. The remaining columns contain the other two orientations, with every fourth polyhedron having one orientation and the remainder having the other orientation.

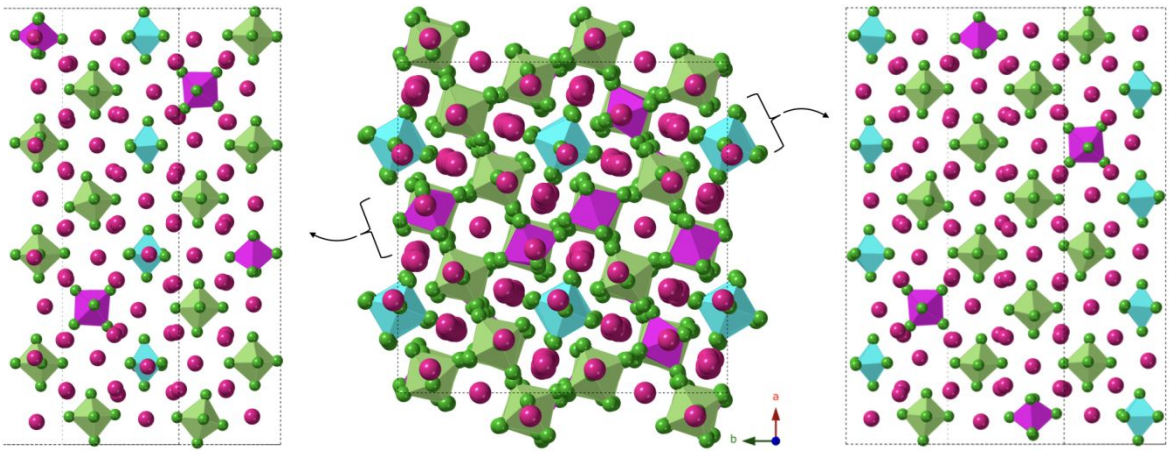

Figure 5. Structure of *t*-Rb_3GaF_6 showing the view down the *c*-axis and two individual planes of polyhedra. Rb atoms are shown in pink, the three different orientations of Ga polyhedra in blue, pink and green, and F atoms in green.

Thermal Behavior

Rb_3AlF_6 was previously reported to undergo a phase transition to a cubic structure upon heating.[7] DSC data were collected on all four compounds, shown in Figure 6 and summarized in Table 3, and the other three compounds were found to also exhibit structure transitions. To confirm the nature of these transitions, high temperature PXRD data were collected. Waterfall plots showing the PXRD patterns upon heating and cooling for Cs_3AlF_6, Cs_3GaF_6, and Rb_3GaF_6 are shown in Figures 7 and S2-S6 and confirm the conversion to a cubic structure at high temperatures. These structure transitions are at 291.2 °C for Cs_3AlF_6, 367.6 °C for Cs_3GaF_6, and 365.6 °C for Rb_3AlF_6. Unlike the other three phases, which all undergo a single high temperature structure transition, Rb_3GaF_6 undergoes two transitions at lower temperatures, 86.6 and 106.9 °C, prior to converting to cubic at 397.2 °C. A similar set of three transitions are observed upon heating α-K_3AlF_6, which is isostructural with *t*-Rb_3GaF_6. Upon heating, α-K_3AlF_6 transforms to β-K_3AlF_6, a second tetragonal phase with space group I4/m, then to γ-K_3AlF_6, which is analogous to the *o*-A_3MF_3 phases reported here, and finally to the cubic phase, δ- K_3AlF_6.[6] The higher temperature

intermediate phase of Rb_3GaF_6 is analogous to γ-K_3AlF_6. While the structure could not be refined due to the greatly altered peak intensities arising from the furnace attachment to the UltimaIV diffractometer, the lattice parameters were refined using the Rigaku SmartLab Studio II software,[24] and found to be $a = 37.959(4)$ Å, $b = 12.6368(12)$ Å, and $c = 17.9872(12)$ Å at 225 °C. Interestingly, the lower temperature intermediate polymorph of Rb_3GaF_6 is not analogous to β-K_3AlF_6, see Figure S7. Structure solution was not possible due to the highly complex nature of the structure and the lack of SCXRD quality crystals. PXRD patterns of the two intermediate polymorphs are provided in Figures S7 and S8.

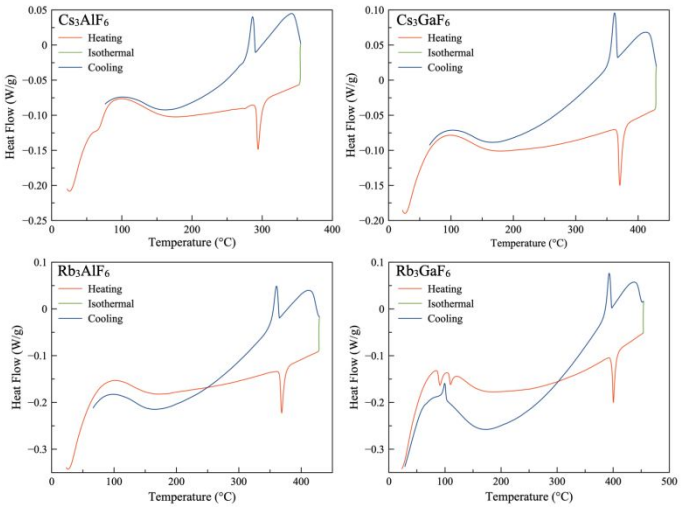

Figure 6. DSC data for the four compounds showing the heat flow as a function of temperature. Endothermic peaks point down and exothermic peaks point up. No appreciable difference was observed between the monoclinic and orthorhombic Cs_3MF_6 compounds so only one is shown.

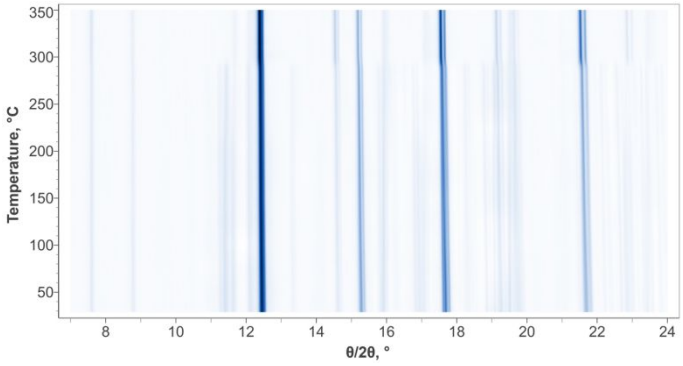

Figure 7. Waterfall plot of the change in PXRD pattern (Mo K_α) upon heating for Cs_3AlF_6, highlighting the structure transition from *m*-Cs_3AlF_6 to *c*-Cs_3AlF_6 at 291.2 °C.

The high temperature cubic structure of Cs_3AlF_6 was determined via high temperature SCXRD, and the high temperature cubic structure of Cs_3GaF_6 was determined via Rietveld refinement of high temperature PXRD data, Figure 8. The high temperature polymorph of Rb_3GaF_6 was confirmed to have the same cubic structure as the other analogues, Figure S9, but Rietveld refinement was not possible due to the greatly altered peak intensities arising from the furnace attachment to the UltimaIV diffractometer. However, the lattice parameters were able to be refined using the cell refinement function in Jade. All three structures crystallize as double perovskites with half the octahedral sites being occupied by the M atom and half by the alkali cation, shown in Figure 9, and lattice parameters a = 9.3433(3) Å for Cs_3AlF_6 at 350 ºC, a = 9.4478(3) Å for Cs_3GaF_6 at 400 ºC, and a = 9.0432(4) Å for Rb_3GaF_6 at 475 ºC.

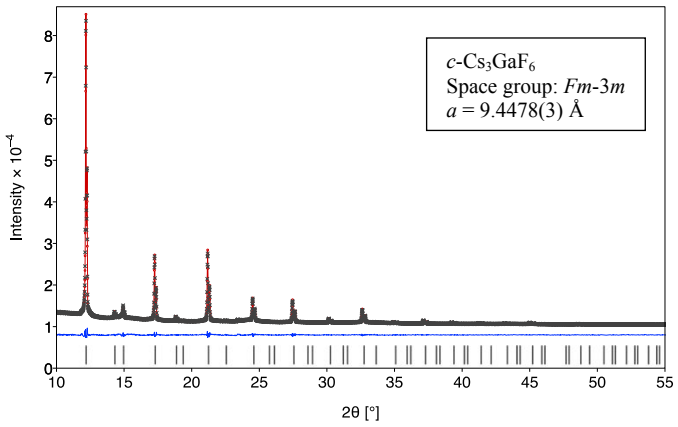

Figure 8: Rietveld refinement plot of Cs_3GaF_6 at 400 °C; red line is Rietveld fit, black X's are observed PXRD (Mo K_α), blue line is residual, and vertical black ticks are allowed Bragg reflections.

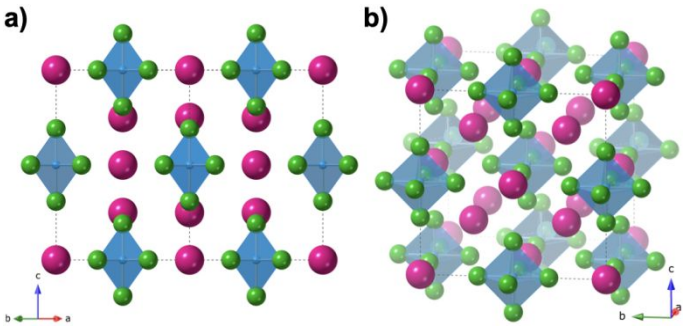

Figure 9. Structure of *c*-Cs_3AlF_6 showing a) the view down the [1 1 0] direction and b) a view highlighting the double perovskite nature of the structure. Cs atoms are shown in pink, Al polyhedra in blue, and F atoms in green.

Table 3. Thermal data for the reported compounds.

Compound[a]	Phase Change T (°C)		Melting Point/
	Heating	Cooling	Decomp. T (°C)[b]
Cs_3AlF_6	291.2	290.0	731
Cs_3GaF_6	367.6	366.5	n.d.[c]
Rb_3AlF_6	365.6	364.6	818
Rb_3GaF_6	86.6	-	907 (decomp.)
	106.9	102.5	
	397.2	397	

[a]No appreciable difference was observed between the monoclinic and orthorhombic Cs_3MF_6 compounds and they are therefore not listed separately
[b]Temperatures provided are melting temperatures unless otherwise indicated
[c]Not determined – Sample exhibited appreciable sublimation prior to melting/decomposing

Simultaneous TGA/DSC data were also collected on each analogue to observe the high temperature melting or decomposition of the phases, shown in Figure S10-S13 and included in Table 3. Cs_3AlF_6 and Rb_3AlF_6 melt at 731 ºC and 818 ºC, respectively, determined visually post-heating. PXRD data collected afterwards showed the refrozen melt to remain A_3AlF_6, indicating congruent melting. Rb_3GaF_6 does not melt but instead decomposes in two steps beginning at 907 °C. The PXRD pattern of the decomposition products could not be indexed using the JCPDF database. Cs_3GaF_6 began to exhibit substantial sublimation starting at 600 ºC, losing 5% mass by 750 ºC without exhibiting any sign of melting or decomposition. The sample was not heated further so as to prevent damage to the instrument.

Polymorphism in Cs_3MF_6

Two low temperature polymorphs of Cs_3AlF_6 and Cs_3GaF_6 are observed: *m*-Cs_3MF_6 and *o*-Cs_3MF_6. The driving force behind which polymorph forms is unclear. While reactions heated to 600 °C typically produce the monoclinic polymorph and reactions heated to 750 °C typically produce the orthorhombic polymorph, on rare occasions, 600 °C reactions were observed to form the orthorhombic phase instead. While the synthesis temperature appears to influence the ultimate room temperature polymorph, neither phase exists at the synthesis temperatures, with the products of both temperature reactions presumably forming as the cubic phase and then converting to the observed polymorphs after the flux has frozen during cooling. Heating ground samples of the monoclinic polymorphs in the TGA above the cubic transition temperature resulted in the orthorhombic phase upon cooling. TGA on single crystals of the monoclinic phases also resulted in the orthorhombic polymorph for Cs_3AlF_6 upon cooling, but for Cs_3GaF_6, the sample reverted back to the monoclinic polymorph. Similarly, quenching single crystals from above the cubic transition temperature, heated in evacuated fused silica tubes and quenched in either water or liquid nitrogen, resulted in *m*-Cs_3GaF_6 and *o*-Cs_3AlF_6. The driving forces behind the formation of the monoclinic or orthorhombic polymorphs are clearly quite subtle and we were unable to come up with any conclusive reasoning for which phase forms.

During their syntheses, all products were cooled at the same rate through their structure transitions from the high temperature cubic polymorphs to the low temperature polymorphs. Therefore, it does not appear that the polymorph formation is kinetically driven. We did, however, attempt to determine which polymorph is the thermodynamically stable polymorph. Polycrystalline samples of each polymorph of Cs_3MF_6 were sealed in evacuated, dried Pyrex tubes and annealed for 72 h at 50 °C below the temperature at which they convert to the cubic polymorph.

While the *o*-Cs_3MF_6 samples did not change, the two *m*-Cs_3MF_6 samples converted to the orthorhombic polymorph, suggesting that *o*-Cs_3MF_6 is the thermodynamically stable polymorph.

Conclusions

The flux crystal growth method was adapted for the crystal growth of fluorides by utilizing fluoride reagents and mixed alkali chloride/fluoride fluxes in sealed silver tubes. This allowed for the single crystal growth of A_3MF_6 (A = Rb, Cs; M = Al, Ga). For Cs_3AlF_6 and Cs_3GaF_6, two polymorphs were observed at room temperature, *m*-Cs_3MF_6 and *o*-Cs_3MF_6. For the two Rb containing compositions, only one room temperature polymorph was observed, *o*-Rb_3AlF_6 and *t*-Rb_3GaF_6, respectively. Simultaneous TGA/DSC and high temperature SCXRD/PXRD were used to study the high temperature behavior of A_3MF_6. The compounds of all four compositions were found to undergo structure transitions upon heating to the same cubic structure type, *c*-A_3MF_6.

Conflicts of Interest

There are no conflicts of interest to declare.

Acknowledgements

Research was supported by the U.S. National Science Foundation under grants DMR-2221403 and DMR-1806279. NSF's ChemMatCARS is supported by the Divisions of Chemistry (CHE) and Materials Research (DMR), National Science Foundation, under grant number NSF/CHE-1834750. Use of the Advanced Photon Source, an Office of Science User Facility operated for the U.S. Department of Energy (DOE) Office of Science by Argonne National Laboratory, was supported by the U.S. DOE under Contract No. DE-AC02-06CH11357.

Supporting Information

A comparison of the two models for *m*-Cs_3GaF_6, waterfall plots showing the change in PXRD pattern during heating and cooling for each compound, PXRD data for the three high temperature polymorphs of Rb_3GaF_6, TGA data for each compound, Rietveld refinement plots for each refined compound, and room temperature PXRD data for each compound.

Accession Codes

CCDC 2193505-2193510 (SCXRD) and 2193514-2193516 (PXRD) contain the supplementary crystallographic data for this paper. The second model for *m*-Cs_3GaF_6 is CCDC 2239383. These data can be obtained free of charge via www.ccdc.cam.ac.uk/data_request/cif, or by emailing data_request@ccdc.cam.ac.uk, or by contacting The Cambridge Crystallographic Data Centre, 12 Union Road, Cambridge CB2 1EZ, UK; fax: +44 1223 336033.

References

1. Haupin, W. E., Electrochemistry of the Hall-Heroult process for aluminum smelting. *J. Chem. Educ.* **1983,** *60*, 279.
2. Tyagi, A. K.; Köhler, J., Preparation and rietveld refinement of the structure of β-Li_3AlF_6. *Mater. Res. Bull.* **1997,** *32*, 1683-1689.
3. Burns, J. H.; Tennissen, A. C.; Brunton, G. D., The crystal structure of α-Li_3AlF_6. *Acta Crystallogr. B* **1968,** *24*, 225-230.
4. Abakumov, A. M.; Rossell, M. D.; Alekseeva, A. M.; Vassiliev, S. Y.; Mudrezova, S. N.; Van Tendeloo, G.; Antipov, E. V., Phase transitions in K_3AlF_6. *J. Solid State Chem.* **2006,** *179*, 421-428.
5. Abakumov, A. M.; King, G.; Laurinavichute, V. K.; Rozova, M. G.; Woodward, P. M.; Antipov, E. V., The crystal structure of α-K_3AlF_6: Elpasolites and double perovskites with broken corner-sharing connectivity of the octahedral framework. *Inorg. Chem.* **2009,** *48*, 9336-9344.
6. King, G.; Abakumov, A. M.; Woodward, P. M.; Llobet, A.; Tsirlin, A. A.; Batuk, D.; Antipov, E. V., The high-temperature polymorphs of K_3AlF_6. *Inorg. Chem.* **2011,** *50*, 7792-7801.
7. Rakhmatullin, A.; Šimko, F.; Véron, E.; Allix, M.; Martineau-Corcos, C.; Fitch, A.; Fayon, F.; Shakhovoy, R. A.; Okhotnikov, K.; Sarou-Kanian, V.; Korenko, M.; Netriová, Z.; Polovov, I. B.; Bessada, C., X-ray diffraction, NMR studies, and DFT calculations of the room and high temperature structures of rubidium cryolite, Rb_3AlF_6. *Inorg. Chem.* **2020,** *59*, 6308-6318.
8. Holm, J. L., Phase transitions and structure of the high-temperature phases of some compounds of the cryolite family. *Acta Chem. Scand.* **1965,** *19*, 261-263.
9. Ming, H.; Zhang, J.; Liu, L.; Peng, J.; Du, F.; Ye, X., Luminescent properties of a $Cs_3AlF_6:Mn^{4+}$ red phosphor for warm white light-emitting diodes. *ECS J. Solid State Sci. Technol.* **2018,** *7*, R149-R155.
10. Köhler, J.; Tyagi, A. K., Crystal structure of ß-lithium hexafluorogallate, Li_3GaF_6. *Z. Kristallogr. - New Cryst. Struct.* **1999,** *214*, 25-26.
11. Massa, W.; Rüdorff, W., On α- and β-Li_3MeF_6 compounds. *Z. Naturforsch. B* **1971,** *26*, 1216-1218.
12. Yeon, J.; zur Loye, H.-C., Hydrothermal synthesis and crystal structure of hexafluorogallate, Na_3GaF_6. *J. Chem. Crystallogr.* **2017,** *47*, 129-132.
13. Rawat, P.; Kumar Saroj, S.; Gupta, M.; Vijaya Prakash, G.; Nagarajan, R., Wet-chemical synthesis, structural characterization and optical properties of rare-earth doped halo perovskite K_3GaF_6. *J. Fluorine Chem.* **2017,** *200*, 1-7.
14. King, G., New examples of non-cooperative octahedral tilting in a double perovskite: phase transitions in K_3GaF_6. *Acta Crystallogr. B* **2020,** *76*, 789-794.
15. Scholz, G.; Korup, O., High-energy ball milling—a possible synthesis route for cryolite and chiolite. *Solid State Sci.* **2006,** *8*, 678-684.
16. Song, Q.; Liu, Z.; Jiang, H.; Luo, Z.; Sun, P.; Liu, G.; Liu, Y.; Jiang, H.; Jiang, J., The hydrothermally synthesis of $K_3AlF_6:Cr^{3+}$ NIR phosphor and its performance optimization based on phase control. *J. Am. Ceram. Soc.* **2021,** *104*, 5235-5243.

17. Bäucker, C.; Becker, P.; Morell, K. J.; Niewa, R., Novel fluoridoaluminates from ammonothermal synthesis: Two modifications of K_2AlF_5 and the elpasolite Rb_2KAlF_6. *Inorganics* **2022,** *10*, 7.
18. APEXIII Version 2016.5-0, SAINT Version 7.60A, SADABS Version 2016/2; Bruker Analytical X-ray Systems: Madison, Wisconsin, USA, 2016.
19. Sheldrick, G., SHELXT - Integrated space-group and crystal-structure determination. *Acta Crystallogr. A* **2015,** *71*, 3-8.
20. Sheldrick, G., A short history of SHELX. *Acta Crystallogr. A* **2008,** *64*, 112-122.
21. Dolomanov, O. V.; Bourhis, L. J.; Gildea, R. J.; Howard, J. A. K.; Puschmann, H., OLEX2: a complete structure solution, refinement and analysis program. *J. Appl. Crystallogr.* **2009,** *42*, 339-341.
22. Spek, A., Single-crystal structure validation with the program PLATON. *J. Appl. Crystallogr.* **2003,** *36*, 7-13.
23. Hubschle, C. B.; Sheldrick, G. M.; Dittrich, B., ShelXle: a Qt graphical user interface for SHELXL. *J. Appl. Crystallogr.* **2011,** *44*, 1281-1284.
24. *SmartLab Studio II*, 4.5.286.0; Rigaku: 2021.
25. Bugaris, D. E.; zur Loye, H.-C., Materials discovery by flux crystal growth: Quaternary and higher order oxides. *Angew. Chem. Int. Ed.* **2012,** *51*, 3780-3811.
26. Klepov, V. V.; Juillerat, C. A.; Pace, K. A.; Morrison, G.; zur Loye, H.-C., "Soft" alkali bromide and iodide fluxes for crystal growth. *Front. Chem.* **2020,** *8*, 518-518.
27. Kanatzidis, M. G.; Pöttgen, R.; Jeitschko, W., The metal flux: A preparative tool for the exploration of intermetallic compounds. *Angew. Chem. Int. Ed.* **2005,** *44*, 6996-7023.
28. Wanklyn, B. M., The flux growth of crystals of some fluorides (AlF_3, CrF_3, NiF_2, $KNiF_3$, CoF_2 and $KCoF_3$). *J. Cryst. Growth* **1969,** *5*, 279-283.
29. Wanklyn, B. M., Flux growth of crystals of some transition metal fluorides. *J. Mater. Sci.* **1975,** *10*, 1487-1493.
30. Wanklyn, B. M.; Wondre, F. R.; Maqsood, A.; Yanagisawa, K.; Davison, W., Flux growth of crystals of some transition metal fluorides. *J. Mater. Sci.* **1979,** *14*, 1447-1456.
31. Wanklyn, B. M.; Wondre, F. R.; Garrard, B. J.; Cermak, J.; Davison, W., Flux growth of crystals of some transition metal fluorides. *J. Mater. Sci.* **1981,** *16*, 2303-2309.
32. Coles, R. E., The permeability of silver to oxygen. *Br. J. Appl. Phys.* **1963,** *14*, 342-344.
33. Morrison, G.; Ramanantoanina, H.; Urland, W.; Smith, M. D.; zur Loye, H.-C., Flux synthesis, structure, properties, and theoretical magnetic study of uranium(IV)-containing $A_2USi_6O_{15}$ (A = K, Rb) with an intriguing green-to-purple, crystal-to-crystal structural transition in the K analogue. *Inorg. Chem.* **2015,** *54*, 5504-5511.
34. King, G.; Abakumov, A. M.; Hadermann, J.; Alekseeva, A. M.; Rozova, M. G.; Perkisas, T.; Woodward, P. M.; Van Tendeloo, G.; Antipov, E. V., Crystal structure and phase transitions in Sr_3WO_6. *Inorg. Chem.* **2010,** *49*, 6058-6065.